Arch. Metall. Mater. **63** (2018), 2, 953-961

DOI: 10.24425/122427

D. PIETRAS*, T. SADOWSKI*#

PARAMETRIC STUDY OF GEOMETRY EFFECT ON RESPONSE TO APPLIED LOADINGS OF METALLIC HONEYCOMB STRUCTURES BY VIRTUAL TESTING OF MESOSCALE MODELS

In this paper were conducted virtual tests to assess the impact of geometry changes on the response of metallic hexagonal honeycomb structures to applied loadings. The lateral compressive stress state was taken into consideration. The material properties used to build numerical models were assessed in laboratory tests of aluminium alloy 7075. The modelling at meso-scale level allow to comprehensive study of honeycomb internal structure. The changes of honeycomb geometry elements such as: fillets radius of the cell edges in the vicinity of hexagonal vertexes, wall thickness were considered. The computations were conducted by using finite element method with application of the ABAQUS finite element method environment. Elaborated numerical models allowed to demonstrate sensitivity of honeycomb structures damage process response to geometry element changes. They are a proper tools to perform optimization of the honeycomb structures. They will be also helpful in designing process of modern constructions build up of the considered composite constituents in various branches of industry. Moreover, the obtained results can be used as a guide for engineers. Conducted virtual tests lead to conclusion that simplification of the models of internal honeycomb structure which have become commonplace among both engineers and scientist can lead to inaccurate results.

Keywords: Virtual testing, Aluminium hexagonal honeycomb, Compression behaviour, Quasi-static, Deformation, Effective elastic property, Buckling, Collapse

1. Introduction

The sandwich structures are widely used in aerospace industry due to the fact that they allow to construct lighter and mechanically beneficial structural parts. In these type of composites the stiff skins are separated by lightweight honeycomb core which increases the moment of inertia. In the role of the cores of sandwich structures are used polymeric foams [1,2] and honeycomb structures. Their main role in composite structures is to carry the shear loads in plane and normal loads out of plane from composite skins. The special case of loadings are low-velocity impacts [3]. Their big advantage is high impact energy absorption capacity. The dynamic analyses of aircraft honeycomb sandwich structures was done in [4,5]. Nowadays, this feature can be improved by creation of hierarchical honeycomb structures which are constructed by replacing each vertex of a traditional hexagonal honeycomb with a smaller hexagonal topology and repeating this process for constructing fractal-appearing honeycombs with higher order of structural hierarchy [6]. In case of blast loadings the stepwise graded cores are very promising [7]. The way to improve the sandwich structures lifetime is filling of honeycomb type cores with foam, it allows to enhance the damage resistance to debonding propagation [8].The structures with local face-core interface damage are considered in [9,10]. In the structural part of aircraft subjected to vapor condensation process the closed cell honeycomb cores can be not suitable due to the fact that accumulated water can increase the weight and reduce the mechanical properties the honeycomb cell materials such an NOMEX. On this field of structure development the new generation of sandwich cores called “folded cores” or “origami like cores” was introduced, [11,12]. Development of modern manufacturing techniques like additive manufacturing reduces the current limitations in geometry of cores [13].

The research of each variation of composite internal structure involves a large amount of specimen testing to investigate the achieved effect. The time and cost of this process can be reduced by using the virtual testing technique. Therefore, the Finite Element Method (FEM) has become most commonly used tool in the development process of the internal structures of aircraft composites.

Described fields of honeycomb structures development require improvement of their modelling method. The numerical methods still provides more accurate solutions both in macro-scale modelling of sandwich structures [14] and in meso-scale modelling. Therefore, this fact they are a proper tool to predict mechanical and thermal properties of the cores before their manufacturing. It’s allows to perform accurate optimisation process to achieve demanded mechanical characteristic of the composites.

* POLITECHNIKA LUBELSKA, 20-618 LUBLIN, 40 NADBYSTRZYCKA STR., POLAND

Corresponding author: t.sadowski@pollub.pl

Literature survey leads to the conclusions that despite of substantial development of numerical simulations in the last two decades many authors treat as negligible the geometrical imperfections such as: non zero radius of fillets in corrugated sheets of aluminium walls. Figure 1 presents the microscopic image of exemplary real extruded honeycomb panel. This panel contains cells 4.3×3.0 mm. The measurement performed on this specimen indicate that mean fillet radius R is equal to 0.286 mm. This problem was partially mentioned in [15]

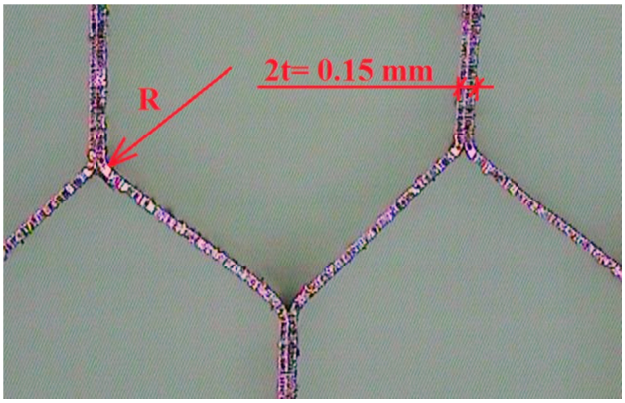

Fig. 1. Microscopic image of real aluminium honeycomb structure

Therefore, this study is aimed to explain the effect of geometry simplifications including different:

- thickness' of honeycomb walls t and
- different fillet radius R

on the mechanical response of the honeycomb structure. Moreover, the relationships between the effective properties such as out of the plane modulus of elasticity E_z, critical compressive load F_{max} and geometrical parameters such as the wall thickness t and the fillets radius R were assessed.

2. Assessment of the aluminium alloy 7075 properties

The response of honeycomb structures to applied loadings may be strongly influenced by cell wall material mechanical properties. Therefore, in the performed calculations the accurate material model was employed.

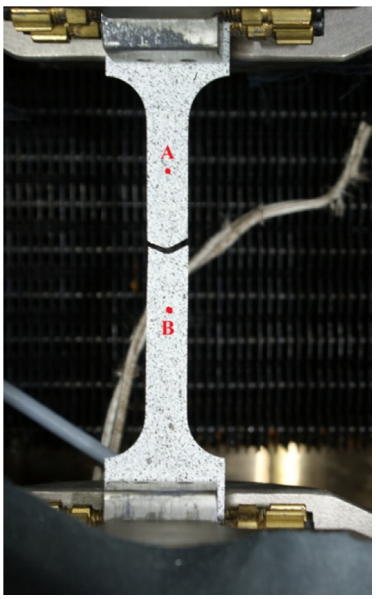

Fig. 2 The tension test setup with dot pattern for the DIC system ARAMIS

The material data were assessed using flat specimen made of aluminium alloy 7075 with cross section 10×2 mm, which were subjected to the uniaxial tensile test performed on the MTS 810 testing machine, Fig. 2. The deformations field were measured by Digital Image Correlation (DIC) system ARAMIS.

The uniaxial tensile test was performed with constant displacement rate conditions. In order to describe degradation process of this material a scalar damage parameter $D^{(n)}$ was estimated, which was related to the elastic response during deformation history. In order to measure values of the $D^{(n)}$ a loading-unloading-reloading (LUR) cycles with gradual increase of displacement (Fig. 3) was programmed in MultiPurpose TestWare application of the Flex Test software prepared by MTS. The rate of displacement was equal to 0.003 mm/min for loading and unloading cycles. The typical relation of normal stress σ_{11} on the strains ε_{11} acquired during the tests is plotted in Fig. 3.

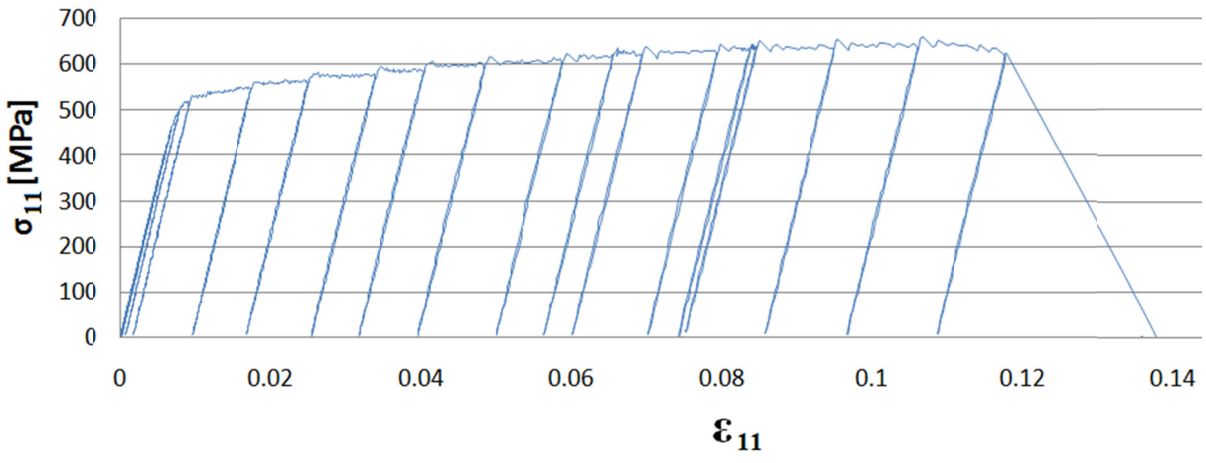

Fig. 3. The loading-unloading-reloading (LUR) test of the considered aluminium alloy

The normal stress σ_{11} was calculated by dividing the applied load by initial cross section of the specimen A. The normal strains ε_{11} were calculated by dividing the displacement increment Δ of the segment AB (Fig. 1) by the base length $|AB|$:

$$\sigma_{11} = \frac{F}{A}, \quad \varepsilon_{11} = \frac{\Delta|AB|}{|AB|} \tag{1}$$

Application of the ABAQUS code for numerical solution of the mechanical response of the honeycomb sandwich structures made of metallic material requires definition of the plastic and hardening properties as functions of true stress σ_t and plastic strain ε_{pl} expressed by:

$$\sigma_t = \sigma_{11}(1 + \varepsilon_{11}) \tag{2}$$

$$\varepsilon_t = \ln(1 + \varepsilon_{11}) \tag{3}$$

$$\varepsilon_{pl} = \varepsilon_t - \frac{\sigma_t}{E_0} \tag{4}$$

The value of the scalar damage parameter $D^{(n)}$ is defined for the n-th LUR cycle as:

$$D^{(n)} = 1 - \frac{E^{(n)}}{E_0} \tag{5}$$

where $E^{(n)}$ is modulus of elasticity in (n) unloading cycle of the test, while E_0 is modulus of elasticity in first unloading cycle ($n = 1$). The base elastic parameters were determined by: $E_0 = 71.502$ GPa and $v_o = 0.346$. These initial elastic properties were used in elastic region of material response in honeycomb panels analyses. Figure 6 shows the distribution of the $D^{(n)}$ corresponding to residual plastic strain ε_t^{res} which corresponds to the end of each unloading process in cycle (n), Fig. 4.

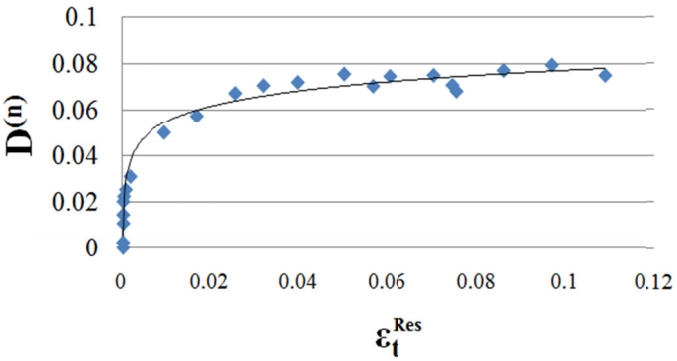

Fig. 4. Damage parameter $D^{(n)}$ as function of residual plastic strain ε_t^{res}

Approximation of experimental results can be done with the help of the following logarithmic function:

$$D^{(n)}(\varepsilon_{pl}^{res}) = 0.00967145743950258 \ln(\varepsilon_{pl}^{res}) + 0.09922410686608280 \tag{6}$$

which is valid for the room temperature.

3. Virtual testing of honeycomb panels under compression along the honeycomb walls

A geometry of the honeycomb structure and its basic parameters are shown in Fig. 5. In this paper we investigated change of hexagonal vertex radius (Fig. 1) in range: $R = 0$ mm; 0.25 mm; 0.50 mm; 0.75 mm and 1.00 mm. Moreover, for each filet radius we analysed 4 different wall thickness $t = 0.025$ mm; 0.050 mm; 0.075 mm and 0.1 mm. The height of considered honeycomb structures is equal to $h = 12.7$ mm, whereas the cross sectional area of the specimens loaded in virtual compressive tests is equal to $A_{HC} = 13.568*25.659$ mm $= 348.142$ mm^2.

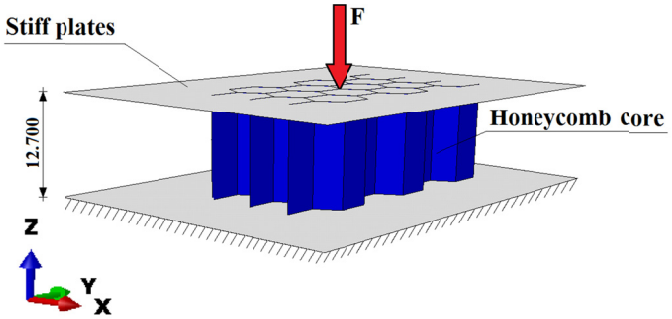

Fig. 5. The virtual compression test conditions

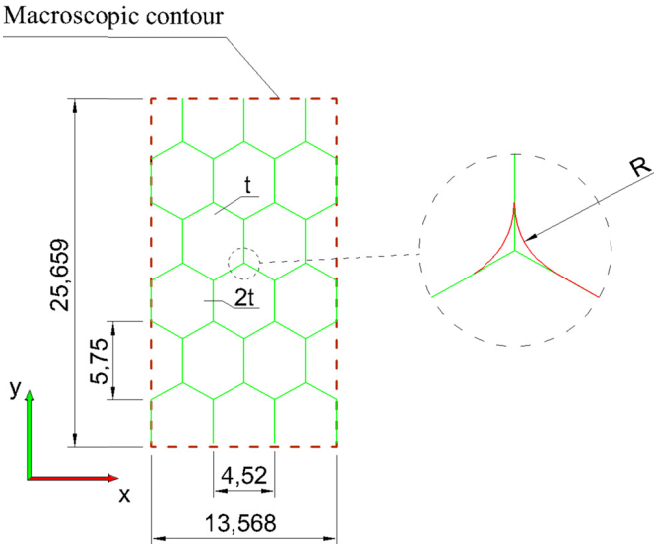

Fig. 6. Dimensions and geometrical parameters of the considered honeycomb panels

The classical honeycomb structure is manufactured by printing the adhesive strips on the material ribbons in staggered pattern, stacking the material ribbons, curing the adhesive under pressure and elevated temperature. At the final stage of manufacturing the prepared structure is expanded to form hexagonal honeycomb. Another way to manufacture the honeycomb structures is assembling previously corrugated sheets [16]. In the consequence of this manufacturing process in places where the ribbons are joined the thickness of wall is doubled (see Figs. 1 and 6).

In the literature, there are many approaches concerning choosing the proper size of the representative volume element (RVE) in modelling of the honeycomb structures, which should be taken into account in numerical calculations. For example in [17] authors used one hexagonal shape cell, but in [18] a fragment of the cell with Y shape was applied. The comprehensive study performed in [18] proved that both large and small domains like one unit cell and 4×4 cells gave identical initial collapse responses up to the second load peak. The differences between the responses of the various domains start during formation of the second fold. The laboratory tests performed with real specimens lead to conclusion that stable results for elastic properties of honeycomb cores may be achieved, when not smaller sample than 13×13 cells were used [19]. In the present study we used a fragment of the honeycomb structure as shown in Fig. 7.

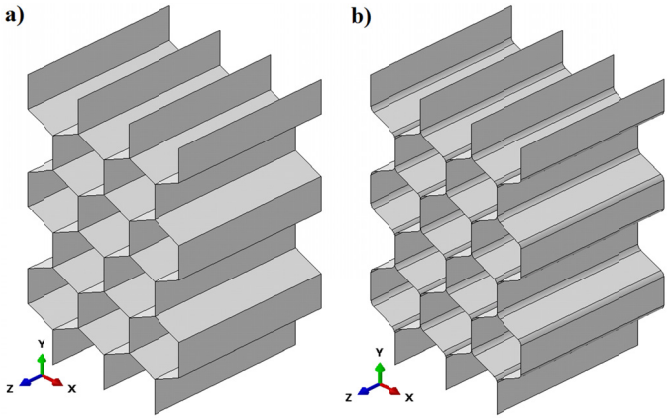

Fig. 7. The analysed honeycomb RVE with different filled radii a) $R = 0$ b) $R = 0.75$ mm

To perform the flatwise compression test conditions [20] we analysed the honeycomb RVE loaded by two rigid plates, Fig. 5. The edges of the honeycomb cells are tied to the plates surfaces. The bottom plate has fixed all degrees of freedom while the top plate has enforced uniform displacement in $-Z$ direction.

Every real honeycomb structure has geometrical and material imperfections which leads to reduction of the effective mechanical properties. Moreover, the honeycomb structure contains adhesive joints between the ribbons. An example of imperfections as debonding of the adhesive joints in the honeycomb sandwich made of the NOMEX core was presented in [20].

Different techniques how to incorporate structural imperfections into numerical models are described in [21]. They are include:

- a node shaking,
- a random material property assignment,
- a pre-buckled cell walls

The other modern approaches how to include in the FEM analysis:

- geometrical imperfections due to manufacturing process,
- material imperfections such as Young modulus,
- changes of the walls thickness

were presented in [17]. All imperfections can be included in the model by defining of different elastic constants and cell wall thickness for each finite element according to a pre-defined field based on statistical distributions of these quantities. These statistical distributions of geometric parameters variation are estimated using a 3D-photo-scanning and CT-scanning.

In this paper imperfections were taken into account by change the nodes coordinates in relation to the perfect geometry on the base the displacements obtained in buckling analyses. The first ten buckling modes were superposed onto unit cell's mesh and scaled to 10% the wall thickness. The geometry of the first and the 100 buckling modes of considered structures are presented in Fig. 8. Table 1 contains eigenvalues corresponding to the elastic buckling loads.

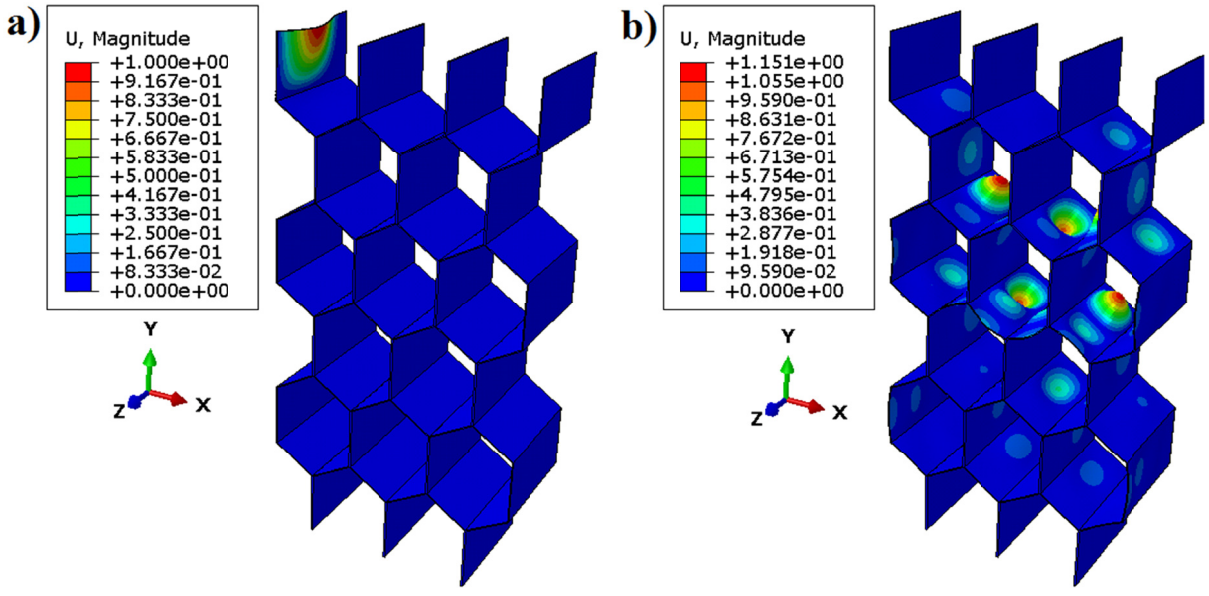

Fig. 8. Buckling modes of the considered honeycomb structures for the: a) mode 1 and b) mode 100

The results summarized in Table 1 indicate that the elastic eigenvalues are strongly depended on the fillet radius R. The first eigenvalue decrease whereas the higher eigenvalues increases when the fillet radius is higher. In case of the thin-walled honeycomb panels (t = 0.025 mm) the relative difference between the first buckling loads is equal to 5.5%, whereas, in the thick-walled panels (t = 0.1 mm) this difference is equal to 14%.

TABLE 1

Eigen values η: 1, 50 and 100 for considered honeycomb panels

R [mm]	T [mm]	η_1	η_{50}	η_{100}
0.00	0.025	**70.394**	194.750	210.260
	0.050	552.440	1551.700	1674.300
	0.075	1824.300	5203.700	5607.400
	0.100	**4221.600**	12227.00	13148.000
0.25	0.025	**66.747**	202.790	219.700
	0.050	527.740	1576.100	1680.600
	0.075	1751.700	5190.800	5536.000
	0.100	**4054.300**	11983.000	12831.000
0.50	0.025	**64.132**	234.660	250.650
	0.050	502.220	1704.700	1848.900
	0.075	1664.200	5447.300	5996.600
	0.100	**3865.200**	12321.000	13261.000
0.75	0.025	63.859	284.840	302.660
	0.050	499.420	1943.400	2161.800
	0.075	1665.500	5903.100	6779.400
	0.100	**3893.000**	13251.000	15265.000
1.00	0.025	**64.754**	349.740	351.280
	0.050	485.660	2274.500	2358.400
	0.075	1592.400	6522.200	7020.400
	0.100	**3686.800**	13904.000	15087.000

As illustrative examples several numerical virtual tests (Fig. 5) were performed for quasi-static compression analyses using ABAQUS/EXPLICITE. The honeycomb cells are discretized using S4 – a fully integrated 4 node doubly curved general purpose shell finite elements (FE). The mesh convergence studies performed in [22] indicates that convergence was achieved when the FE size is equal to 0.2 mm for the cell dimensions 4.2×3.2 mm. In conclusion, the authors suggest to use FE of the size 0.4 mm for a good trade-off between convergence and computational effort. The similar results were achieved in [6]. In the present study to achieve good representation of curved faces in the vicinity of the hexagonal vertexes the square FE with approximate mesh dimension 0.1 mm were used. For very small fillet radius, i.e. R = 0.25 mm, the constraint was build to divide the corner into not less than 8 FE.

In contrast to the purely elastic response and initial post-buckling process crushing process due to compression of the honeycomb panels involves local bending and self-contact between the internal structure constituents. Therefore the EXPLICITE codes are the best for mesoscale modelling of the honeycomb structures. The computational time in ABAQUS/EXPLICITE quasi-static analyses can by reduced by mass scaling, what allows to increase the time increment. To speed up calculation procedure in this study the mass was scaled by factor 1e4, which increased the time increment hundred-fold. Nevertheless, the kinetic energy remains only small fraction of the strain energy as shown in Fig. 9.

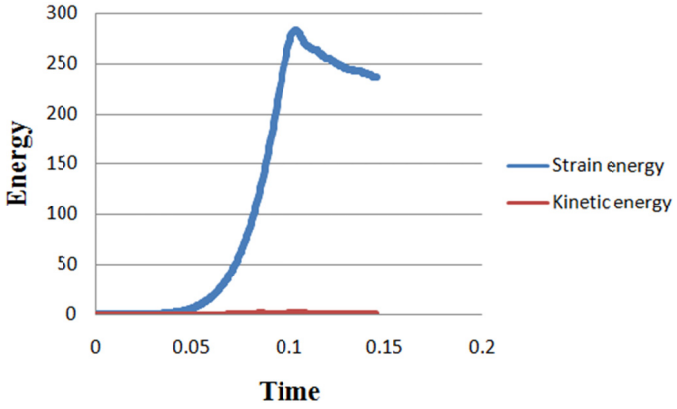

Fig. 9. Comparison of the strain energy to kinetic energy in quasi-static analyses of the honeycomb panels response

4. Numerical results of the compression tests

The compression test (Fig. 5) was continued to the final failure. Figures 10,11 present deformed shape and calculated stress distributions at failure stage of deformation process. Both figures are related to the internal honeycomb structure with the walls thickness t = 0.05 mm. In Fig. 10, when the fillet radius of the structure R = 0 mm we can observe an ordered pattern of efforted and not efforted regions. In the vicinity of hexagonal vertexes levels of the Huber-von Mises reduced stresses are higher than the yield stress σ_y. For the internal structure of the honeycomb with R = 1 mm (Fig. 11) we observed much larger areas of yielded zones.

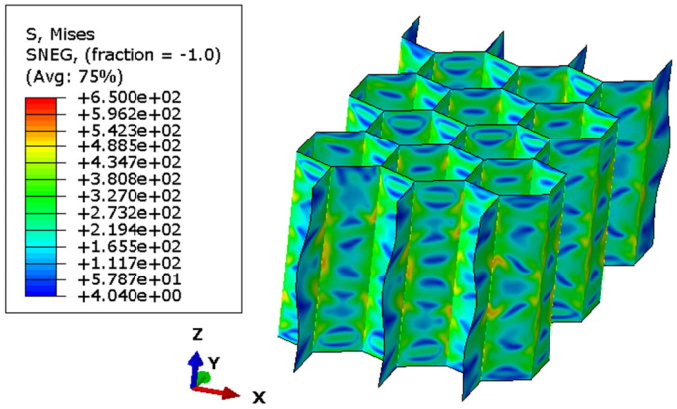

Fig. 10. Huber-von Mises reduced stress distribution in the honeycomb structure with R = 0 mm

The behaviour of the analysed fragments of the structures (Figs. 6,7), subjected to compression, are presented in Figs. 12-15. F_z is the reaction force while U_z is the displace-

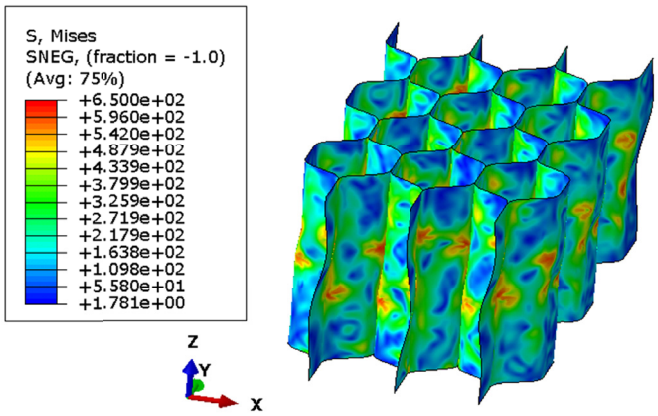

Fig. 11. Huber-von Mises reduced stress distribution in the honeycomb structure with R = 1 mm

ment in vertical Z direction (Figs. 10,11). The obtained load-displacement curves include three regions:

- a linear part at the beginning of loading process,
- a nonlinear part until the force reach the local maximum,
- in the last region the load tend to reach plateau stress in the structure.

In Fig. 12 we can observe strong impact of the fillet radius R on derived critical loading of the structure. The strongest critical force was achieved for structure with R = 0 mm. Difference between this case and typical structure with R = 0.25 mm is equal to 26.547%.

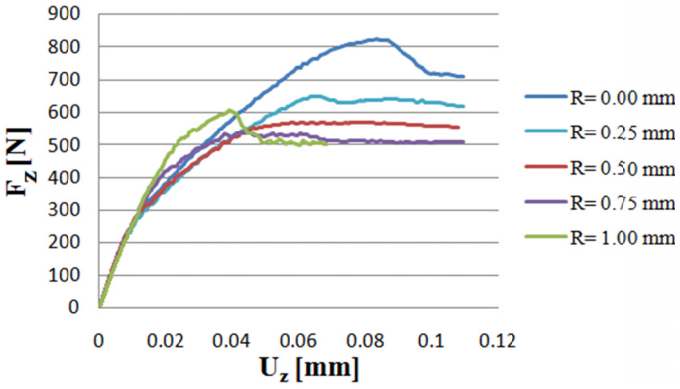

Fig. 12. Response of the honeycomb panels (with t = 0.025 mm) to applied deformation process

In case of two times thicker walls in the considered honeycomb, i.e. for t = 0.05 mm (Fig. 13) the effect of the fillet radius R change is smaller. The difference between the internal structure with R = 0 mm and for the case with R = 0.25 mm is equal to 8.921%.

The virtual compression tests done with the honeycomb structure built of ribbons having 0.075 mm thickness indicate the smallest sensitivity of their load-displacement characteristic in relation to the parameter R. The relative difference between the critical load for R = 0 mm and R = 0.25 mm is equal to 3.5%. Despite of this fact the early post-buckling paths are significantly different for structures with various values of the fillet radius R.

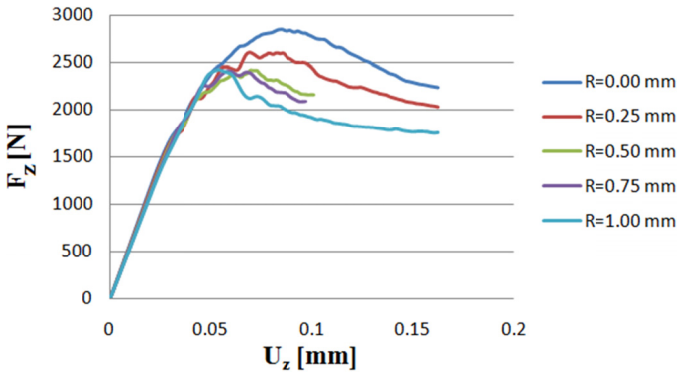

Fig. 13. Response of the honeycomb panels (with t = 0.05 mm) to applied deformation process

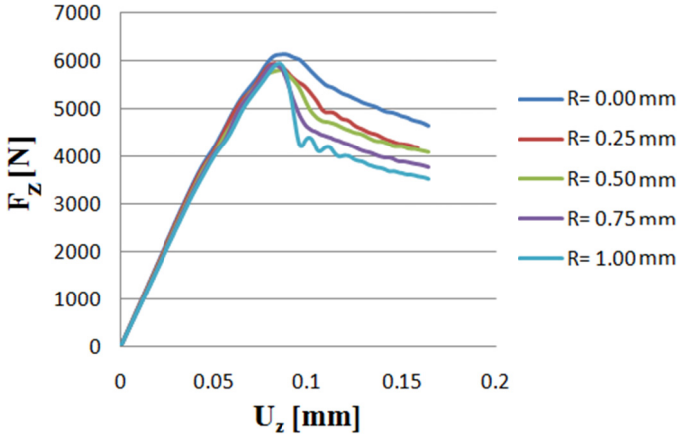

Fig. 14. Response of the honeycomb panels (with t = 0.075 mm) to applied deformation process

For the thick honeycomb cores in the panels with very thick aluminium walls of order t = 0.1 mm once again the strong influence of R was observed. The relative difference between critical loads in cases R = 0 mm and R = 0.25 mm is equal to 11.372%.

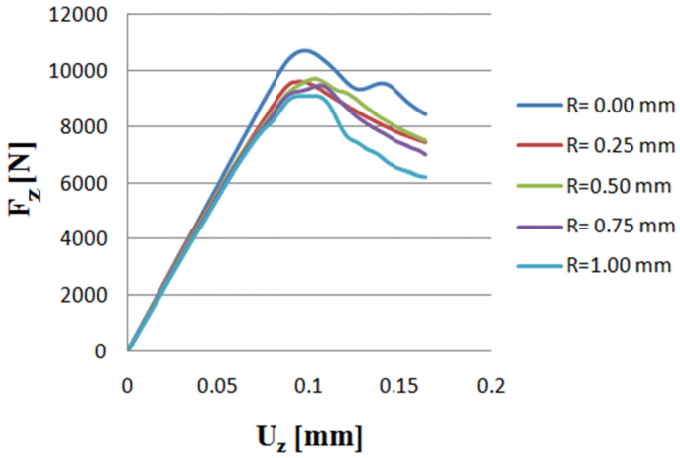

Fig. 15. Response of the honeycomb panels (with t = 0.10 mm) to applied deformation process

Summarizing, in each considered case of the honeycomb internal structure we observed strong influence of the fillet ra-

dius R on the mechanical response of the sandwich subjected to compressive deformation. The highest sensitivity was indicated for the honeycomb structures with thinnest walls.

Conducted numerical tests allow also to estimate values of the effective elastic modulus E_z in the analysed structures in Z direction (Figs. 5,6). This value is defined as a ratio between the stress increment $\Delta\sigma_z = \Delta F_z/A_{HC}$ and the strain increment $\Delta\varepsilon_z = \Delta U_z/h$. The increments are computed in linear parts of the load-displacement curve. The obtained values of E_z are collected in Table 2, which contains the critical values of the compressive forces $F_{\max}$ and critical equivalent macroscopic stresses $\sigma_{\max}$ achieved during the virtual tests of the analysed honeycomb panels.

TABLE 2

Quasi-static virtual compression test results for the honeycomb panels

t [mm]	R [mm]	$F_{\max}$ [N]	$\sigma_{\max}$ [MPa]	E_z [MPa]
0.025	0.00	822.480	2.362	1051.021
	0.25	649.939	1.867	1031.087
	0.5	605.988	1.741	1015.056
	0.75	540.338	1.552	999.4782
	1.00	605.812	1.740	986.468
0.050	0.00	2846.150	8.175	2180.756
	0.25	2613.040	7.506	2135.748
	0.5	2427.450	6.973	2087.603
	0.75	2407.840	6.916	2049.735
	1.00	2426.060	6.969	2017.012
0.075	0.00	6160.170	17.694	3272.783
	0.25	5950.800	17.093	3214.112
	0.5	5826.560	16.736	3143.454
	0.75	5919.500	17.003	3084.048
	1.00	5947.100	17.082	3033.396
0.100	0.00	10716.100	30.781	4383.247
	0.25	9621.860	27.638	4290.569
	0.5	9732.470	27.955	4203.088
	0.75	9488.020	27.253	4124.311
	1.00	9133.480	26.235	4055.589

The effective modulus of elasticity E_z exhibit a dependency on the fillet radius R parameter, but the effect is not so substantial as in case of the critical load. The relative difference of the values E_z between two cases for $R = 0$ mm and for $R = 0.25$ mm is close to 2% and is practically not independent of the wall thicknesses t. The total change of the E_z values in the considered range of the fillet radius R form 0 up to 1 mm not exceeds 10%.

The data gathered in Table 2 indicate also, that the relation $E_z(R)$ in considered range is almost linear. An exemplary relation for the honeycomb panel with $t = 0.075$ mm is plotted in Fig. 15. The linear fitting of relations $E_z(R)$ for the each considered honeycomb panel can be performed with good correlation coefficient R^2. Estimated relations are presented below:

$$E_z(R) = \begin{cases} -64.2859 \cdot R + 1048.7538\big|_{t=0.025\,\text{mm}} \\ -165.4004 \cdot R + 2176.8710\big|_{t=0.05\,\text{mm}} \\ -243.5352 \cdot R + 3271.3262\big|_{t=0.075\,\text{mm}} \\ -328.6294 \cdot R + 4375.6754\big|_{t=0.100\,\text{mm}} \end{cases} \tag{7}$$

Moreover, relationship of the effective modulus of elasticity with respect to the cell wall thicknesses t computed for $R = 0.025$ mm is also linear:

$$E_z(t) = 43429.7151\, t - 46.3163\big|_{R=0.025} \tag{8}$$

Theoretical relations of effective elastic properties of hexagonal honeycomb panels in plane $x\,y$, (Fig. 11) are presented in [23].

5. Conclusion

The purpose of this paper was to perform several numerical tests in order to estimate the influence of geometrical parameters of the honeycomb core on the mechanical response of the sandwich structures. The numerical quasi-static compressive deformation processes at meso-scale were performed. Moreover,

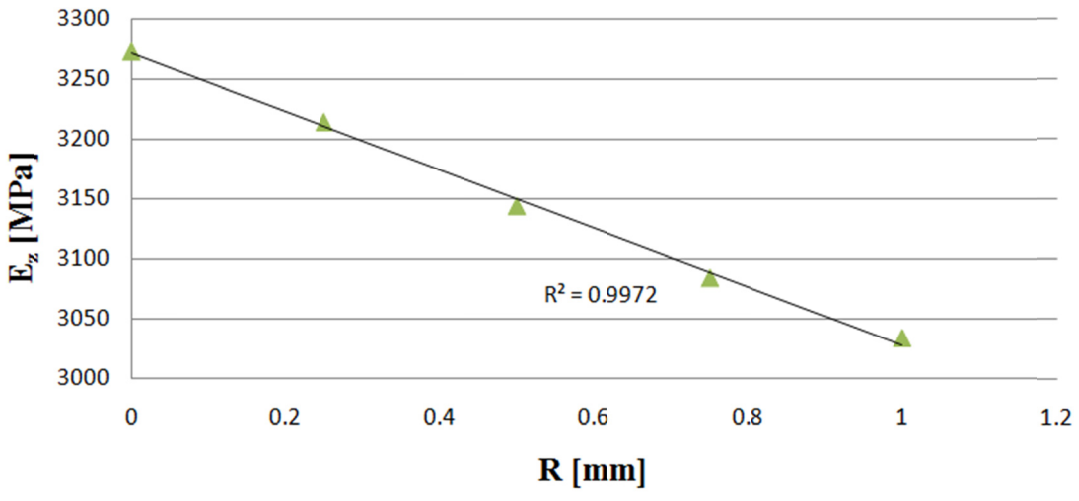

Fig. 16. Effect of the fillet radius R value on the effective Young modulus E_z of the honeycomb core with the wall thickness equal to $t = 0.075$ mm

the experimental tests of the honeycomb core material – the aluminium alloy 7075 – were performed. The results of these tests were used to assess the honeycomb cells properties and further to calibrate the FEM models. Based on performed numerical calculations the following conclusions can be drown:

- The fillet radius R and the wall thickness t parameters strongly influence the honeycomb core response in the sandwich structures.
- The strongest critical forces was achieved for idealised structures with $R = 0$ mm.
- The highest difference between critical forces derived between cases $R = 0$ mm and $R = 0.25$ mm equal to 26.547% was achieved for honeycomb with thinnest walls $t = 0.25$ mm.
- The smallest sensitivity to the R changes occurred in the sandwich structures with the honeycomb wall thickness $t = 0.75$ mm.
- Increase of the R parameter lead to decreasing the effective elastic honeycomb properties and the critical force in compressive stress state.
- The dependence of the effective young modulus along Z direction in relation to R is linear. The difference between cases of the fillet radius 0 mm and $R = 0.25$ mm is close to 2% for each considered wall thicknesses.

Further investigations are necessary to analyse impact of the fillet radius value R and the wall thickness t on the honeycomb structures response subjected to shear loadings. Moreover, damage processes leading to cracking (e.g. [25-43]) of the sandwich panels should be taken into account in the next papers.

Acknowledgement

The authors would like to mention that this research has been done within the POLONEZ 2 project, grant agreement No. UMO-2016/21/P/ST8/00790, supported by the National Science Centre of Poland at the Lublin University of Technology within the European Union's Horizon 2020 research and innovation pro-gramme under the Marie Skłodowska-Curie grant agreement No. 665778

REFERENCES

[1] V. Burlayenko, T. Sadowski, Transient dynamic response of debonded sandwich plates predicted with the finite element, Meccanica **49**, 2617-2633 (2014).

[2] V. Burlayenko, T. Sadowski, Nonlinear dynamic analysis of harmonically excited debonded sandwich plates using finite element modeling, Composite Structures **108**, 354-366 (2014).

[3] V. Burlayenko, T. Sadowski, A numerical study of the dynamic response of sandwich plates initially damaged by low-velocity impact, Comput. Mat. Sci. **52**, 212-216 (2012).

[4] V. Burlayenko, T. Sadowski, Simulations of Post-impact Skin/core Debond Growth in Sandwich Plates Under Impulsive Loading, Journal of Applied Nonlinear Dynamics **3**, 369-379 (2014).

[5] T. Sadowski, J. Bęc, Effective properties for sandwich plates with aluminium foil honeycomb core and polymer foam filling – Static and dynamic response, Computational Material Science **50**, 1269-1275 (2011).

[6] G. Sun, H. Jiang, J. Fang, G. Li, Q. Li, Crashworthiness of vertex based hierarchical honeycombs in out-of-plane impact, Materials and Design **110**, 705-719 (2016).

[7] S. Li, X. Li, Z. Wanga, G. Wu, G. Lu, L. Zhao, Finite element analysis of sandwich panels with stepwise graded aluminum honeycomb cores under blast loading, Composites: Part A **80**, 1-12 (2016).

[8] V. Burlayenko, T. Sadowski, Analysis of structural performance of aluminium sandwich plates with foam-filled hexagonal foam, Comp. Mater. Sci. **45**, 658-662 (2009).

[9] V. Burlayenko, T. Sadowski, Finite element nonlinear dynamic analysis of sandwich plates with partially detached face-sheet and core, Finite Elements in Analysis and Design **62**, 49-64 (2012).

[10] V .Burlayenko, T. Sadowski, Influence of skin/core debonding on free vibration behaviour of foam and honeycomb cored sandwich plates, Int. J. Non-Linear Mechanics **45**, 959-968 (2010).

[11] J.M. Gattas, Z. You, Design and digital fabrication of folded sandwich structures, Automation in Construction **63**, 79-87 (2016).

[12] X. Zhou, H. Wang, Z. You, Mechanical properties of Miura-based folded cores under quasi-static loads, Thin-Walled Structures **82**, 296-310 (2014).

[13] R. Hedayati, M. Sadighi, M. Mohammadi-Aghdama, A.A. Zadpoor, Mechanical properties of additively manufactured octagonal honeycombs, Materials Science and Engineering C **69**, 1307-1317 (2016).

[14] V.N. Burlayenko, H. Altenbach, T. Sadowski, An evaluation of displacement-based finite element models used for free vibration analysis of homogeneous and composite plates, Journal of Sound and Vibration **358**, 152-175 (2015).

[15] R. Seemann, D. Krause, Numerical Modeling of Nomex Honeycomb Sandwich Cores at Meso-Scale Level, Composite Structures **159**, 702-718 (2017).

[16] N. Haydn, G. Wadley, Multifunctional periodic cellular metals, Phil. Trans. R. Soc. A **364**, 31-68 (2006).

[17] D. Asprone, F. Auricchio, C. Menna, S. Morganti, A. Prota, A. Reali, Statistical finite element analysis of the buckling behavior of honeycomb structures, Composite Structures **105**, 240-255 (2013).

[18] A. Wilbert, W.-Y. Jang, S. Kyriakides, J.F. Floccari, Buckling and progressive crushing of laterally loaded honeycomb, International Journal of Solids and Structures **48**, 803-816 (2011).

[19] T. Jin, Z. Zhou, Z. Wang, G. Wu, X. Shu, Study on the effects of specimen in-plane size on the mechanical behavior of aluminum hexagonal honeycombs, Materials Science & Engineering A **635**, 23-35 (2015).

[20] L. Liu, P. Meng, H. Wang, Z. Guan, The flatwise compressive properties of Nomex honeycomb core with debonding imperfections in the double cell wall, Composites Part B **76**, 122-132 (2015).

[21] S. Heimbs, Virtual testing core structures using dynamic finite elements simulations, Computational Material Science **45**, 205-216 (2009).

[22] R. Seemann, D. Krause, Numerical modelling of nomex honeycomb cores for detailed analyses of sandwich panel joints 11th World Congress on Computational Mechanics (WCCM XI) Jully 20-25 2014 – Barcelona, Spain.

[23] Q. Kepeng, W. Zhi, Z. Weihong, The effective elastic properties of flexible hexagonal honeycomb cores with consideration for geometric nonlinearity, Aerospace Science and Technology **58**, 258-266 (2016).

[24] Q. Kepeng, W. Zhi, Z. Weihong, The effective elastic properties of flexible hexagonal honeycomb cores with consideration for geometric nonlinearity, Aerospace Science and Technology **58**, 258-266 (2016).

[25] T. Sadowski, E. Postek, C. Denis, Stress distribution due to discontinuities in polycrystalline ceramics containing metallic inter-granular layers, Comp. Mat. Sci. **39**, 230-236 (2007).

[26] L. Marsavina, T. Sadowski, Kinked cracks at a bi-material ceramic interface – numerical determination of fracture parameters, Comp. Mat. Sci. **44**, 941-950 (2009).

[27] T. Sadowski, P. Golewski, The influence of quantity and distribution of cooling channels of turbine elements on level of stresses in the protective layer TBC and the efficiency of cooling, Comp. Mater. Sci. **52**, 293-297 (2012).

[28] T. Sadowski, P. Golewski, Detection and numerical analysis of the most efforted places in turbine blades under real working conditions, Comp. Mater. Sci. 64, 285-288 (2012).

[29] L. Marsavina, T. Sadowski, Fracture parameters at bi-material ceramic interfaces under bi-axial state of stress. Comp. Mater. Sci. **45**, 693-697 (2009).

[30] J. Gajewski, T. Sadowski, Sensitivity analysis of crack propagation in pavement bituminous layered structures using a hybrid system integrating Artificial Neural Networks and Finite Element Method, Comp. Mater. Sci. **82**, 114-117 (2014).

[31] L. Marsavina, T. Sadowski, Stress Intensity Factors for an Interface Kinked Crack in a Bi-Material Plate Loaded Normal to the Interface, Int. J. Frac. **145**, 237-243 (2007).

[32] T. Sadowski, L. Marsavina, Multiscale Modelling of Two-phase Ceramic Matrix Composites. Comp. Mat. Sci. **50**, 1336-1346 (2011).

[33] G. Golewski, P. Golewski, T. Sadowski, Numerical modeling crack propagation under Mode II fracture in plain concretes containing siliceous fly-ash additive using XFEM method. Comp. Mat. Sci. **62**, 75-78 (2012).

[34] T. Sadowski, K. Nakonieczny, Thermal shock response of FGM cylindrical plates with various grading patterns. Comp. Mat. Sci. **43**, 171-178 (2008).

[35] T. Sadowski, S. Samborski, Modelling of porous ceramics response to compressive loading, J. Am. Cer. Soc. **86**, 2218-2221 (2003).

[36] T. Sadowski, S. Samborski, Prediction of mechanical behaviour of porous ceramics using mesomechanical modelling, Comp. Mat. Sci. **28**, 512-517 (2003).

[37] T. Sadowski, L. Marsavina, N. Peride, E.-M. Craciun, Cracks propagation and interaction in an orthotropic elastic material: Analytical and numerical methods, Comp. Mat. Sci. **46**, 687-693 (2009).

[38] K. Nakonieczny, T. Sadowski, Modelling of thermal shock in composite material using a meshfree FEM, Comp. Mater. Sci. **44**, 1307-1311 (2009).

[39] T. Sadowski, S. Samborski, Development of damage state in porous ceramics under compression. Comp. Mat. Sci. **43**, 75-81 (2008).

[40] E. Postek, T. Sadowski, Assessing the influence of porosity in the deformation of metal-ceramic composites, Compos. Interf. **18**, 57-76 (2011).

[41] L. Marsavina, E. Linul, T. Voiconi, T. Sadowski, A comparison between dynamic and static fracture toughness of polyurethane foams, Polymer Testing **32**, 673-680 (2013).

[42] L. Marsavina, E. Linul, D.M. Constantinescu, D. Apostol, T. Voiconi, T. Sadowski, Refinements on fracture toughness of PUR foams, Eng. Fract. Mech. **129**, 54-66 (2014).

[43] H. Dębski, T. Sadowski, Modelling of microcracks initation and evolution along interfaces of the WC/Co composite by the finite element method, Comp. Mat. Sci. **83**, 403-411 (2014).